

# Freeze granulation: Powder processing for transparent alumina applications

Michael Stuer<sup>a,\*</sup>, Zhe Zhao<sup>b</sup>, Paul Bowen<sup>a</sup>

<sup>a</sup> Powder Technology Laboratory, Material Science Institute, Swiss Federal Institute of Technology, CH-1015 Lausanne, Switzerland

<sup>b</sup> Department of Materials and Environmental Chemistry, Arrhenius Laboratory, Stockholm University, SE-10691 Stockholm, Sweden

Available online 26 March 2012

## Abstract

Use of freeze granulated powders is successfully used as an industrially viable alternative to loose powder sintering for transparent polycrystalline alumina (PCA). Freeze granulation with narrow granule size distribution was realized after suspension condition optimization, with very good flowability and regular spherical shapes. The key factors are low viscosity slurries linked to the complex interactions between the organic processing additives and their interaction with dopant ions in solution. Real in-line transmittances (RITs) of 52% were achieved by pulsed electric current sintering (PECS) of dry pressed green bodies from doped granulated powders. This is the first example of a high RIT (>50%) alumina produced from simple dry pressing of a granulated powder. The results indicate that higher granule solid loads and lower organic additive concentrations give better RITs after PECS. Aging of the powder slurry before freeze granulation proves a crucial step for the optical performance of the final transparent PCA.

© 2012 Elsevier Ltd. All rights reserved.

**Keywords:** A. Sintering; C. Optical properties; D. Al<sub>2</sub>O<sub>3</sub>; E. Armor; SPS

## 1. Introduction

The constant effort to improve the mechanical properties of ceramic materials by microstructure refinement and defect reduction has ultimately led to scientific research and development of transparent ceramic materials. More than any mechanical properties, the optical performance relies on defect-free processing to allow full densification and residual porosity elimination.<sup>1–3</sup> In fact, pores are highly efficient scattering centers depending on their size due to the large refractive index difference between the pore and the ceramic bulk material.<sup>4,5</sup> For anisotropic materials such as alumina, microstructural refinement is an additional requirement to reduce inter-granular scattering due to birefringence.<sup>3</sup>

In recent years, many advances have been made in production of transparent ceramics by various processing and sintering strategies.<sup>1,6–14</sup> Mainstream ceramic processing techniques rely either on dry<sup>11,14,15</sup> or wet powder processing [1,6,9,13,16]—both allowing production of highly dense green bodies (GBs), one key factor for transparent ceramics—as

well as on classic sintering followed by hot isostatic pressing (post-HIP) or novel fast sintering techniques. Among the latter, the most popular for transparent ceramics is pulsed electric current sintering (PECS), also known as spark plasma sintering (SPS).<sup>7,8,11,12,14,17–21</sup> In general, powders for these fast sintering techniques have been loose or freeze dried powders<sup>11,14,15,19,20,22</sup> not necessarily well suited to industrial scale production. Whatever the sintering technique used, increasing focus must be put on industrialization aspects, and especially on the green body fabrication method. Wet processing is rather slow and loose powder handling too difficult and possibly hazardous for processing and health aspects, respectively.

To improve the powder flowability and prevent individual particles from becoming airborne, granulation is the classical approach. When well controlled, self-flowing granulated powders allow automated production of highly dense and defect-free green bodies by relatively quick and simple uniaxial or isostatic pressing methods. The main granulation method used in ceramic processing is spray drying,<sup>23–25</sup> with freeze granulation attracting increasing interest.<sup>26,27</sup>

During spray drying, a powder suspension is sprayed into a hot air cyclone.<sup>28</sup> During drying, the droplets shrink to form powder granules. These granules may be more or less spherical and/or hollow depending on the slurry formulation (i.e. powder load and additives) and drying temperature.<sup>25,29</sup> Binder

\* Corresponding author at: MXD 333 Station 12, CH-1015 Lausanne, Switzerland. Tel.: +41 21 693 49 09; fax: +41 21 693 30 89.

E-mail addresses: [michael.stuer@a3.epfl.ch](mailto:michael.stuer@a3.epfl.ch), [Michael.stuer@epfl.ch](mailto:Michael.stuer@epfl.ch) (M. Stuer).

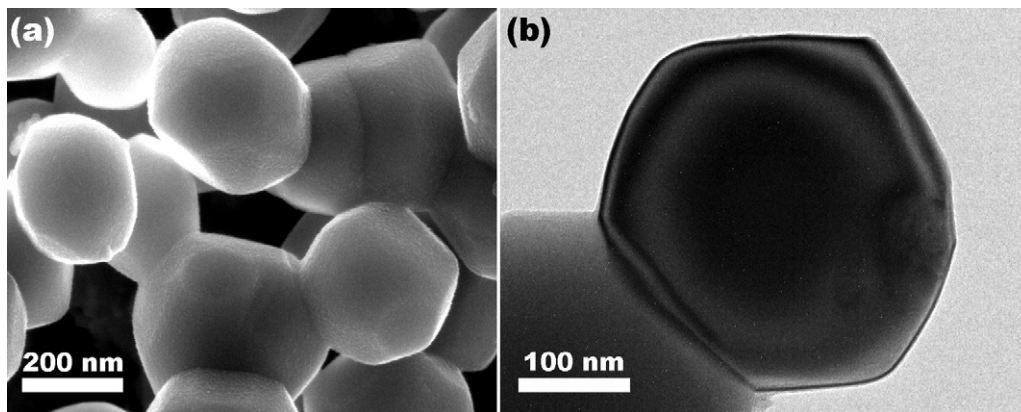


Fig. 1. (a) SEM image and (b) TEM image of the  $\alpha$ - $\text{Al}_2\text{O}_3$  powder used.

migration during the drying can additionally reduce the homogeneity and thereby quality of the granules, leading to inhomogeneities in the green bodies.<sup>30</sup>

Freeze granulation is an alternative to spray drying, solving many of its limitations. During freeze granulation, droplets are rapidly frozen in liquid nitrogen before being recovered and subsequently freeze-dried. Freezing being a fast process, diffusion dynamics are insufficient to induce any binder migration, thereby better preserving the granule homogeneity.<sup>26,27</sup> Additionally, the granules do not shrink during the whole process and therefore maintain their shape and powder density—consequently allowing higher granule deformability compared to spray drying.

In the present study, freeze granulation is explored as an alternative to simple freeze drying for the preparation of transparent polycrystalline alumina (PCA) by PECS in a first step toward a more industrially friendly forming for PCA. The strong dependence of the real in-line transmittance (RIT) on the residual porosity and grain size inhomogeneity makes the RIT an ideal parameter to control the quality of the powder compact. Doped granules with varying solid loads and additives are produced by an experimental setup facilitating control over the granule size and allowing for narrow granule size distributions. As a reference of the granulation performance, the results are compared with those obtained by PECS on the same loose, identically doped and freeze-dried powder. Indeed, use of loose freeze dried powder for PECS has shown promising results with RITs around 56% in an earlier study.<sup>11</sup> That 56% value is only five percent below the expected maximum RIT performance taking into account the particle size of the starting powder, defining the minimal theoretic final grain size. The goal of the study is to show the feasibility and performance of PCA production by simple dry pressing of granulated powders, not yet seen in the literature, compared to reported loose dry or wet green body powder processing techniques.

## 2. Materials and experimental methods

The powder used was a polyhedral near-spherical high-purity  $\alpha$ - $\text{Al}_2\text{O}_3$  (Sumitomo, Japan) with a median particle size  $D_{v,50}$  of 510 nm (Laser diffraction, Mastersizer, Malvern, UK), a total

impurity concentration of less than 0.01 mass% ( $\leq 5$  ppm for Si, Na, Mg, Cu and Fe) and a specific surface  $S_{\text{BET}}$  of  $4.2 \text{ m}^2/\text{g}$  (Fig. 1).

The viscosity of the powder suspension was measured by rheological measurements (RheoStress RS100, Haake, Germany) using a double-gap DIN 53544 concentric cylinder setup. During the rheology measurements, the setup and the slurries were kept at  $25 \pm 0.1$  °C by a thermostatic bath. The data acquisition cycle was: (1) ramp from 0 to  $200 \text{ s}^{-1}$  in 90 s, (2) hold at  $200 \text{ s}^{-1}$  for 60 s, and (3) decrease from 200 to  $0 \text{ s}^{-1}$  in 90 s.

$\zeta$ -Potential measurements (AcoustoSizer II, Colloidal Dynamics, USA) were performed during titration by aqueous dopant-nitrate solutions. The powder was dispersed in 0.005 M  $\text{HNO}_3$  and the pH adjusted by an ammonia solution ( $\text{NH}_4\text{OH}$ ). The total powder solid content was 2.5 wt.% with or without 1 wt.% poly-acrylic acid (PAA) added with respect on the total powder content mass. To avoid interactions between PAA and baseline electrolyte ions, no other salt was added.

To dope the powder and prepare the suspensions for freeze granulation, 50 g of powder was dispersed in ultra-pure water before addition of the desired amounts of a 10 wt.% PAA solution ( $M_w$  2000, pH 9.5) as a dispersant. After an ultrasonic bath (UB) treatment of 15 min,  $\text{Mg}^{2+}$ ,  $\text{Y}^{3+}$  and  $\text{La}^{3+}$  aqueous nitrate solutions (purity >99%, Fluka for La- and Aldrich for Mg- and Y-hexa-hydrated nitrates) were added. The final total dopant level was 450 ppm total cationic ratio (150 ppm for each). Finally, aqueous solutions of polyvinyl alcohol (PVA, Mowiol 4-88, Aldrich) as a binder and polyethylene glycol (PEG,  $M_w$  3000 or 300, Fluka) as a plasticizer were added together with octanol as anti-foaming agent. The final slurries with a pH around 9 were stirred and UB treated for another 15 min before the freeze granulation. The various slurry compositions are summarized in Table 1.

For freeze granulation, the slurry was drawn into a syringe through a  $70 \mu\text{m}$  filter to safely avoid any agglomerates that may obstruct the granulation nozzle. The syringe was then inserted into a syringe pump, shaken periodically throughout the granulation process to avoid PVA segregation, and the freeze granulation process started. The freeze granulation setup (Encapsulator, Inotech Encapsulation AG, Dottikon, Switzerland) is schematically represented in Fig. 2. The slurry droplets are formed by

Table 1

Summary of slurry compositions for freeze granulation, where the wt.% given are compared to the total powder weight in the slurry.

Composition	Total doping [ppm]	Solid load [vol.%]	PAA [wt.%]	PVA [wt.%]	PEG [wt.%]	Octanol [wt.%]
C1	450	25	1	2	1	0.01
C2		30	0.5	1	1	
C3		30	0.5	0.5	0.5	
C4		25	0.5	1	1	
C5		30	0.5	1	0.5	
C6		30	0.5	1	0.5*	
C7		30	0.5	0.5	0.25*	
C8 <sup>+</sup>		30	0.5	0.5	0.5	

\* PEG 300 instead of 3000.

<sup>+</sup> Slurry rolled for 48 h before granulation.

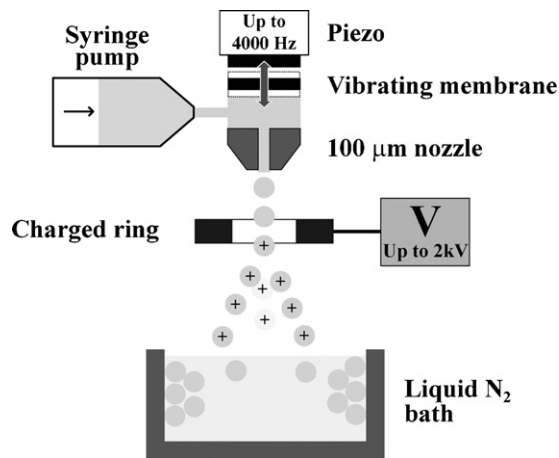


Fig. 2. Schematic representation of the freeze granulation setup. The slurry is pumped with a syringe pump through a nozzle. The droplets are formed by varying the flow rate in the nozzle by a vibrating membrane, and are subsequently charged to avoid recombination before freezing in liquid N<sub>2</sub>. Scaling up can be achieved by the use of multi-nozzle systems.

altering the flow rate through a nozzle with a vibrating membrane. The droplets are subsequently charged in a high voltage ring to avoid recombination during the flight time into the liquid nitrogen bath. For successful granulation, low viscosity slurries are required (<0.25 Pa s at the flow rate used) and the flow through the nozzle has to be laminar (Reynolds number < 2300). Additionally, the powder particle size should be at least eight times smaller than the nozzle diameter to avoid obstruction. In principle, a constant pumping speed could be achieved with a well dispersed powder suspension, allowing for a very narrow droplet size distribution with the final droplet diameter being approximately twice the nozzle diameter.

In the present case, the pumping speed was approximately 1 mL/min, with a membrane vibration frequency of approximately 2 kHz and a ring potential around 1 kV. The exact frequencies and the ring potential were adjusted on a case-by-case basis depending on the pumping speed, the solid load and the organic additives to ensure controlled droplet formation at first and enough charge accumulation later on to avoid recombination. Once suitable parameters are found, they can be kept constant during the whole granulation process as long as a stable pump speed is maintained. After granulation, the granules were loosened from the liquid N<sub>2</sub> container by UB treatment and

subsequently filled into flasks for freeze-drying for approximately 45 h (condenser temperature set to  $-50^{\circ}\text{C}$  at 0.08–0.1 mbar, Alpha 1–4, Christ, Germany).

The flowability of the granules has been estimated from the Carr index ( $I_c$ ) and Hausner ratio ( $R_h$ ):

$$I_c = 100 \frac{\rho_t - \rho_b}{\rho_t} \quad (1)$$

$$R_h = \frac{\rho_t}{\rho_b} \quad (2)$$

where  $\rho_t$  represents the tapped density and  $\rho_b$  the initial brut density of the powder or granules. The flowability is considered excellent if the Carr indices are below 10 and Hausner ratios between 1.00 and 1.11. Their homogeneity was verified on cross sections (SEM, XLF-30, Philips, Netherlands) after resin fixation (EpoFix, Struers, Denmark) by vacuum impregnation.

Green bodies (GBs) were pressed by uniaxial pressing at 150 MPa after re-hydration of the granules for 48 h at 98% relative humidity to ensure plasticity of the granules (0.8 g and 12 mm diameter).<sup>31</sup> No de-molding agent or other lubricant (e.g. oleic acid) was used during the uniaxial pressing.

After binder burnout at  $500^{\circ}\text{C}$  for 5 h, the green body densities were determined geometrically before they were loaded in a graphite die ( $\varnothing$  12 mm), the internal surface of which was covered with a graphite fiber sheet to avoid direct contact between the powder compact and the graphite die. During PECS (Dr. Sinter 2050, Sumitomo Coal Mining Co., Tokyo, Japan) the temperature was measured by an optical pyrometer focused on a small cavity in the graphite die (distance between powder and cavity bottom: 5 mm). The final sintering temperature of  $1350^{\circ}\text{C}$  was reached in 8 min after an initial 3-min hold at  $600^{\circ}\text{C}$  (heating rate approx.  $100^{\circ}\text{C}/\text{min}$ ). The uniaxial pressure ramp was made during the first 2 min of the holding stage at  $600^{\circ}\text{C}$  and kept constant at 100 MPa during the whole sintering cycle. For maximum reproducibility, the sintering temperature and pressure were controlled by automatic controller units. The pulse sequence for all the samples was 12:2 (i.e. 12 on/2 off).

After sintering, the samples were polished down to a thickness of 1 mm with mirror-like parallel surfaces. Optical transmittance measurements of 640 nm light were made with a spectrometer (UV–vis–NIR Lambda 900, Perkin Elmer, USA) in the wavelength range from 300 to 1000 nm. In order to obtain the most reliable RIT values, two metallic shields each with a

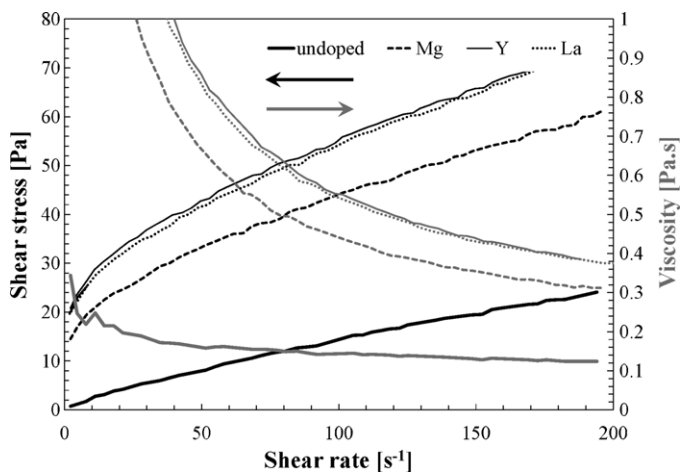


Fig. 3. Effect of dopant addition ( $\text{Mg}^{2+}$ ,  $\text{Y}^{3+}$  and  $\text{La}^{3+}$ ) on the shear stress and viscosity of an alumina powder dispersion in  $\text{HNO}_3$  at pH 4 and 42 vol.% powder load. The cationic dopant concentration for all of the dopants is 0.0065 M (450 ppm cationic ratio).

hole of 4 mm diameter were inserted in the light path to reject extraneous scattered light from reaching the detector.<sup>11</sup> The RIT values given in this paper are calculated for a thickness of 0.8 mm based on the measured 1 mm thick samples in order to best compare with other published RIT results. This is scaled according to Eq. (1):<sup>9</sup>

$$\text{RIT}(t_2) = (1 - R_S) \left( \frac{\text{RIT}(t_1)}{1 - R_S} \right)^{t_2/t_1} \quad (3)$$

where  $\text{RIT}(t_i)$  ( $i = 1, 2$ ) is the RIT for a sample of thickness  $t_i$ .

After the RIT measurements and thermal etching in air at 1150 °C for 30 min (heating rate 10 °C/min), SEM pictures (FEG JSM-7000, JEOL, Japan) were taken for grain size determination. The surface area method was employed applying a correction factor of 1.25.<sup>32,33</sup>

### 3. Results and discussion

#### 3.1. Rheological behavior

To be able to pump and produce granules with narrow granulate size distributions, the powder slurry must meet certain rheological requirements. For undoped powder slurries having a low ionic concentration, the freeze granulation process is straightforward since the granulation viscosity requirement of 0.25 Pa.s taken at  $100 \text{ s}^{-1}$  is easily met (Fig. 3). Although satisfactory optical properties for PCA can be obtained at low temperatures (950 °C) under very high pressure (500 MPa) during the PECS cycle,<sup>7</sup> the stability of these optical properties at high temperatures (e.g. >1000 °C) has not been reported. From our recent work, defect generation and subsequent dislocation climbing producing pores and possible discoloration can only be avoided by using higher sintering temperatures and lower sintering pressures.<sup>11,34</sup> Under these conditions however, powder doping is required in order to inhibit grain growth and achieve a high level of transparency. The dopants were introduced via nitrate solutions, rather than oxides which would avoid increased

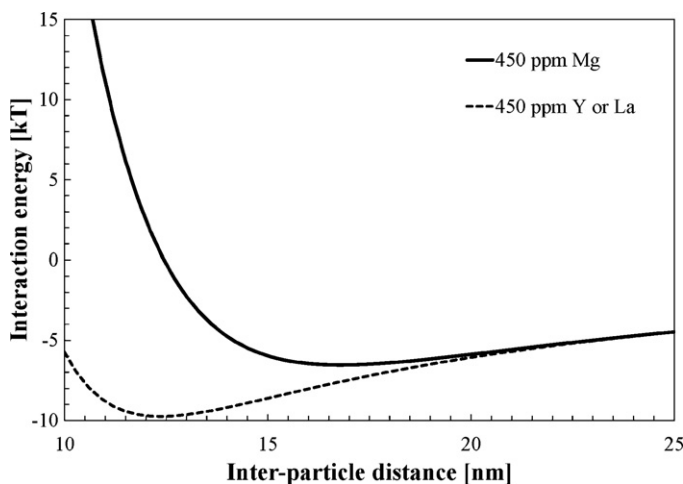


Fig. 4. Secondary minima of the interaction energies for the doped suspensions of Fig. 3. Note that the Y or La interaction energy calculations are identical.

ionic concentrations, in order to ensure sufficient homogeneity to efficiently avoid grain growth and favor densification during the fast PECS cycles.

As illustrated in Fig. 3, the addition of dopants in the form of nitrates at levels as low as 450 ppm total cationic ratio increases the shear stresses and viscosities to values beyond the levels acceptable for the freeze granulation process. This phenomenon is linked to the double layer compression and the reduction of the secondary minimum distance from the interaction energy calculations (Fig. 4). At equal doping levels, higher cation charges (and the additional counter-ion required) compress the double layer and move the secondary minimum toward smaller inter-particle distances. The interaction energy calculations and the rheological behavior are discussed in more detail elsewhere.<sup>35,36</sup> Note that the undoped secondary minimum is not represented in Fig. 4, being at an inter-particle distance much larger than the displayed range (e.g. 50 nm).

In addition to the dopant ionic contribution, the organic additives necessary for proper powder dispersion, granule cohesion, and plasticity also affect the rheological behavior of the powder suspensions (Fig. 5). Shear stress and viscosity results from alumina slurries with PAA only (Fig. 6) show that the viscosity increases at pH 9 compared to pH 4, which may be due to the increased effective volume of the powder by configurational change of the PAA adsorption.<sup>37</sup> In addition, appearance of a yield stress can be observed at pH 9, which is proportional to the effective volume and the solid loading.<sup>35,38</sup>

Upon dopant addition at the desired level for optimal sintering, strong interactions between dissociated PAA with the dopant cations at pH 4<sup>39–41</sup> caused a gel formation, which could not be characterized with the rheological setup. At pH 9 however, no gelation occurred, and the viscosity was low enough for freeze granulation (Fig. 5).

However, hydroxide precipitation may occur at pH 9 depending on the required doping level and solid load, affecting the ionic concentrations and preventing homogeneous powder/granule doping. Taking the maximum ionic dopant concentration of 3.52 mM (from the highest solid load

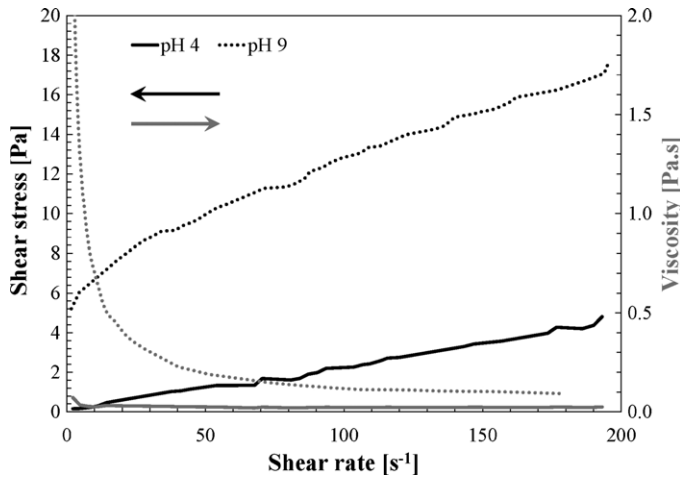


Fig. 5. Shear stress for undoped, 450 ppm  $Mg^{2+}$ - and 450 ppm ( $Mg^{2+}$ ,  $Y^{3+}$ ,  $La^{3+}$ )-doped 30 vol.% alumina slurries. Viscosity is only given for the 450 ppm ( $Mg^{2+}$ ,  $Y^{3+}$ ,  $La^{3+}$ )-doped slurry for the sake of clarity. For all of them, 1 wt.% PAA, 2 wt.% PVA and 1 wt.% PEG compared to the total powder weight were added, representing the highest concentration of organic additives in the granules.

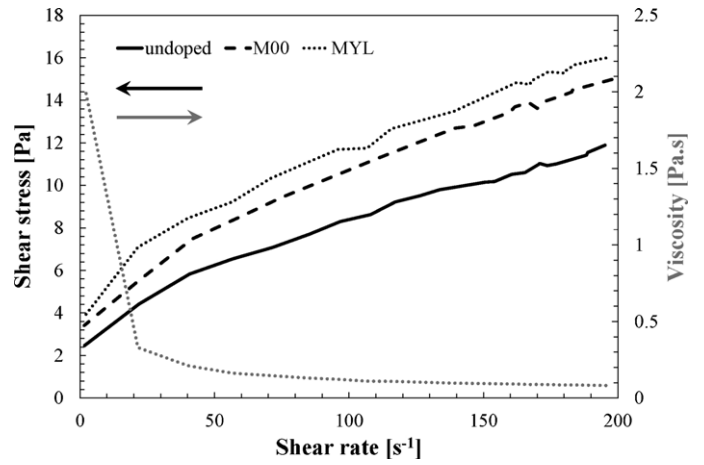


Fig. 6. Effect of pH on shear stress and viscosity of undoped 36 vol.% powder slurries with 0.5 wt.% per powder content PAA added. Increasing pH increases shear stress and viscosity.

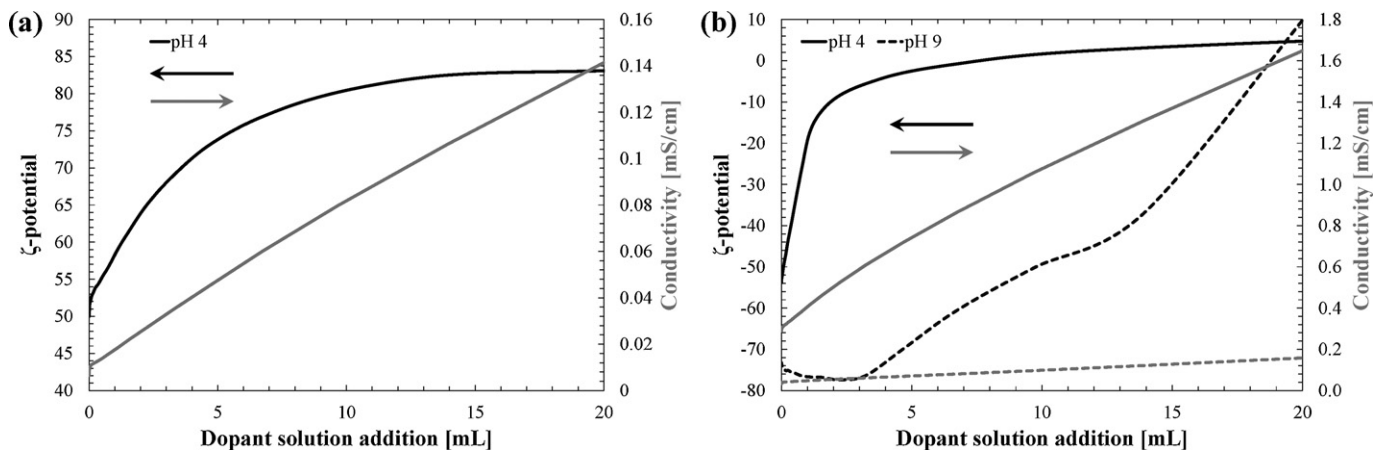


Fig. 7. (a)  $\zeta$ -Potential and conductivity measurements during titration of a 2.5 wt.% alumina slurry with 0.035 M ( $Mg^{2+}$ ,  $Y^{3+}$ ,  $La^{3+}$ )-nitrate solution at equal cationic ratio at pH 4. (b)  $\zeta$ -Potential and conductivity measurements during titration of a 2.5 wt.% alumina slurry containing 1 wt.% PAA (relative to powder weight) with 0.035 M ( $Mg^{2+}$ ,  $Y^{3+}$ ,  $La^{3+}$ )-nitrate solution at equal cationic ratio. The measurements were performed at pH 4 and pH 9.

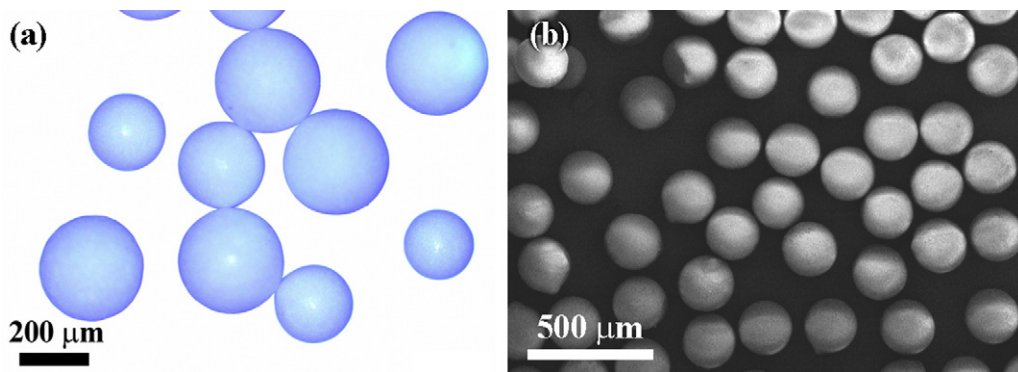


Fig. 8. (a) Optical and (b) SEM image of the final granules. They are all spherical and relatively close in size. The smallest and largest granules (a) form when the frequency and potential values of the encapsulator need adjustment (i.e. improper droplet formation or recombination) because of varying slurry supply flows and/or nozzle obstruction.

powder slurries), the solubility constants for Mg-, Y- and La-hydroxides (e.g.  $K_{sp, Mg(OH)_2} = 5.6E - 12$ ,  $K_{sp, Y(OH)_3} = 1.0E - 22$ ,  $K_{sp, La(OH)_3} = 1.0E - 19$ ) suggest critical pHs at 9.6, 7.5, and 8.5, respectively. Despite these calculated critical pH values, no precipitation could be observed at room temperature in the dispersant liquid at pH 9 before powder addition. This may be explained by possible complex formation between PAA and the dopant cations, decreasing their free ion concentration in solution.<sup>41</sup>

The very different rheological behavior of the powder slurries at pH 4 and pH 9 can also be qualitatively shown by  $\zeta$ -potential measurements (Fig. 7). A sharp increase of the  $\zeta$ -potential occurs at pH 4 with and without PAA added during dopant nitrate titration. At pH 9, the  $\zeta$ -potential remains at first unchanged before it increases more slowly than the pH 4 slurry. The behavior at both pHs is expected to be linked to complex formation between PAA and the cations depending on their relative concentrations and the relative degree of dissociation of the PAA.<sup>41</sup> At pH 4, the degree of dissociation is expected to be around 5%, and at pH 9 around 95%.<sup>42</sup> This explains the rapid change with small amount of dopant ions at pH 4 whereas much higher concentrations of dopants are needed to complex (and neutralize) the almost fully dissociated PAA carboxylate groups at pH 9.

### 3.2. Freeze granulation

The granules obtained from freeze granulation are highly spherical (Fig. 8), as expected unless coagulation occurs during the flight between the droplet formation and the freezing. Broadening of the size distribution can occur because of (1) inhomogeneous flow rates, (2) unstable/inhomogeneous suspensions, and (3) nozzle obstruction. Whereas the first two points require adjustment of the vibration frequency and ring voltage on the freeze granulation apparatus, the latter causes an initial spray formation—, i.e. small droplets of uncontrolled size—before total obstruction occurs. In general, lower viscosities give more homogeneous granule size distributions due to more stable flow rates with the syringe and syringe pump used. Although no fine granule size distribution was evaluated on the total fraction of granules as obtained after granulation, sieving at 100 and 350  $\mu\text{m}$  showed that approximately 70–90 wt.% of the granules had sizes between 100 and 350  $\mu\text{m}$ , and less than 5 wt.% was smaller than 100  $\mu\text{m}$ . To avoid any effect from the larger and smaller fraction of the granules mainly produced during the granulation start and end (i.e. before a steady state was achieved), only the sieved granules between 100 and 350  $\mu\text{m}$  were used for the subsequent dry pressing. The granule size distribution obtained after sieving of the granules from the slurry composition C3 is represented in Fig. 9. Flowability tests with the loose and granulated freeze dried powder confirmed the excellent flowability of the sieved granules as expected from their high sphericity (Fig. 8), with a Carr index less than 5.7 and the Hausner ratio in the range of 1.01–1.06 (Table 2). The granule solid loads have been estimated between 20 and 33 vol.%, by weighing before and after liquid impregnation. This is close to the nominally expected solid loads of 25 and 30 vol.% depending on the slurry composition. Cross-sections show that the granules

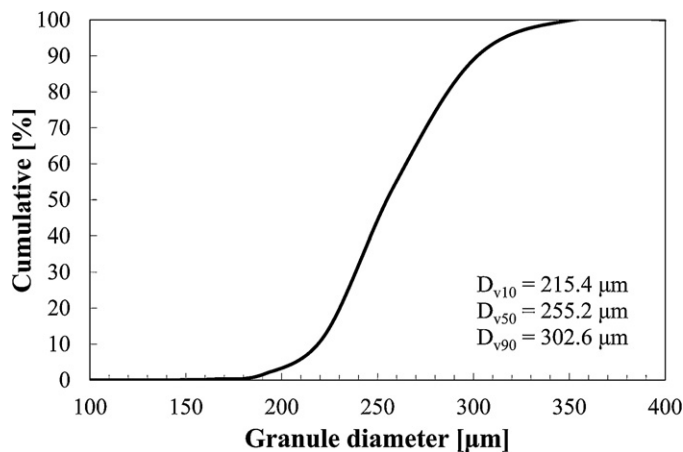


Fig. 9. Granule size distribution of the granule fraction used after sieving (Laser diffraction, Mastersizer, Malvern, UK).

Table 2

Carr indices ( $I_c$ ) and Hausner ratios ( $R_h$ ) for the granules and the freeze dried loose AA04 starting powder. (10) after 10 tapings, (100) after 100 tapings and (100 – 10) after 100 tapings using as initial density the one obtained after 10 tapings.

Composition	Granules	Loose powder
$I_c(10)$	4.9	23.4
$I_c(100)$	5.7	49.8
$I_c(100 - 10)$	0.8	34.4
$R_h(10)$	1.05	1.30
$R_h(100)$	1.06	1.99
$R_h(100 - 10)$	1.01	1.52

are more or less homogeneously filled with powder particles (Fig. 10). A slight radial texturing can be observed from the ice formation during freeze drying, although it is not expected to influence the green body homogeneity. Fracture surfaces showed that the granule structure completely disappears after green body pressing.

### 3.3. Real in-line transmittance

The GB densities after binder burnout and the RITs obtained after PECS of the GBs are summarized in Table 3 for the various slurry compositions used. All the GB densities except for composition C1, which had the highest total organic additive load, are similar and close to 54.3%.

At equal organic additive concentrations (i.e. compositions C2 and C4), increasing the granule solid load from 25 to 30 vol.% seems to have no effect on the GB density, but still increases the RIT from 42.9 to 45.7%. The RITs by PECS being highly reproducible within a range of  $\pm 0.3\%$ ,<sup>11</sup> this observed RIT increase suggests that higher granule solid loads are indeed beneficial, and emphasizes the need for powder slurry optimization to fulfill the granulation requirements.

The effect of PVA and PEG content variations keeping an equal 1:1 ratio, solid load, and PAA content (i.e. compositions C2 and C3 of Table 3) is to increase the RIT with decreasing PVA and PEG content. This may be due residual porosity

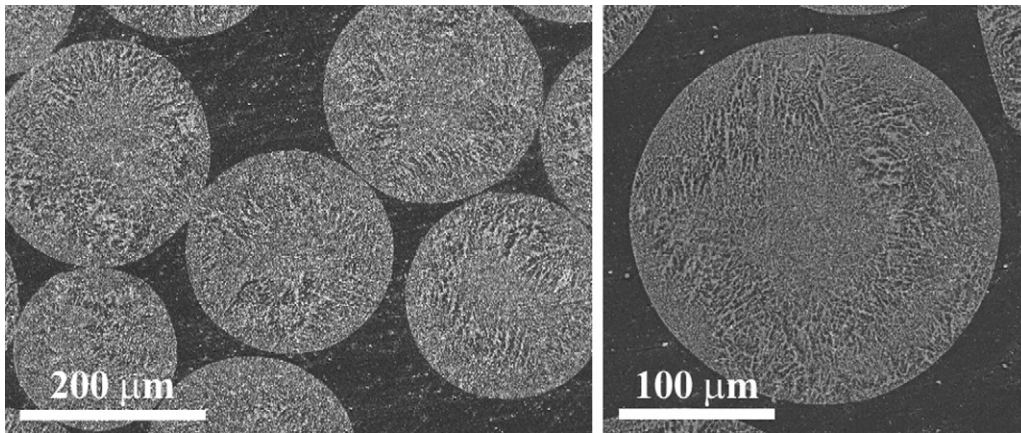


Fig. 10. SEM images of granule cross sections after resin fixation and polishing.

Table 3

Summary of GB densities and RIT results after PECS sintering at 1350 °C and 100 MPa. RIT values are at 640 nm and 0.8 mm thickness.

Composition	Solid load [vol.%]	PVA [wt.%]	PEG [wt.%]	Additives tot. [wt.%]	GB density [%]	RIT [%]
C1	25	2	1	4	53.8 ± 0.3	33.3
C2	30	1	1	2.5	54.4 ± 0.3	45.7
C3	30	0.5	0.5	1.5	54.4 ± 0.3	46.9
C4	25	1	1	2.5	54.5 ± 0.3	42.9
C5	30	1	0.5	2	54.0 ± 0.3	45.3
C6	30	1	0.5*	2	54.3 ± 0.3	43.5
C7	30	0.5	0.25*	1.25	54.6 ± 0.3	45.6
C8 <sup>+</sup>	30	0.5	0.5	1.5	54.6 ± 0.3	51.7

\* PEG 300 instead of 3000.

<sup>+</sup> Slurry rolled for 48 h before granulation.

or carbon residues in the green bodies, even though PVA and PEG are believed to be relatively clean additives.<sup>43,44</sup> Indeed, low amounts of carbon residues may not be noticed for non-transparent ceramic applications for which the highly sensitive RIT is not a metric. This reasoning is indeed supported by earlier findings by Chartier et al.<sup>45</sup> suggesting that at least PVA binder burnout is incomplete up to relatively high temperatures (>800 °C), which cannot be detected by TGA measurements due to insufficient sensitivity. Because of the very low total organic additive amount used during the granulation, such residues could also not be detected using Fourier transform infrared spectroscopy (FTIR, Perkin Elmer, USA) on granules after binder burnout at 500 °C. Indeed the organic peaks before binder burnout are very weak, making it impossible to detect any difference between binder burnout at 500 °C or 800 °C (Fig. 11).

Finally, as expected from earlier findings,<sup>31</sup> the RIT decreases with increasing PVA to PEG ratio. Reducing the PEG content by half at constant PVA content (i.e. compositions C2 and C5 of Table 3) decreases the RIT, with an even more pronounced effect observed when using PEG with lower molecular weight (i.e. C6). Again, although the limited sensitivity of the geometric GB density determination reveals no clear difference before sintering, the RIT results show clear trends which can be linked to the green body processing.

The RITs obtained by uniaxial pressing of loose powder (e.g. simply freeze dried) are 57% under identical doping

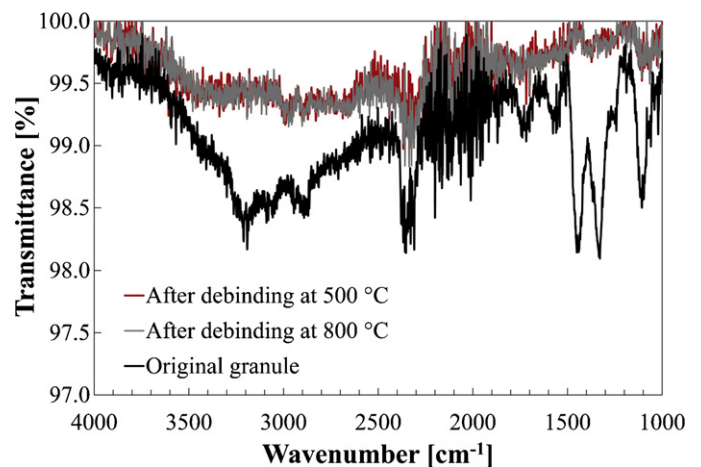


Fig. 11. FTIR spectrum of the original granules, after binder burnout at 500 °C and 800 °C in air for 5 h. The step size of the spectral data acquisition was 2 cm<sup>-1</sup> and 10 scans per sample were done to reduce the noise.

levels and sintering conditions, despite the relatively low GB densities of 53.5 ± 0.3%. This result is 10% better than the best RIT obtained from the granulated powders (i.e. 46.9% for C3) without rolling of the suspension prior to the granulation, even though the grain size distributions are very similar (Fig. 12). Gentle rolling (60 rpm) of the powder suspension C3 (c.f. C8)

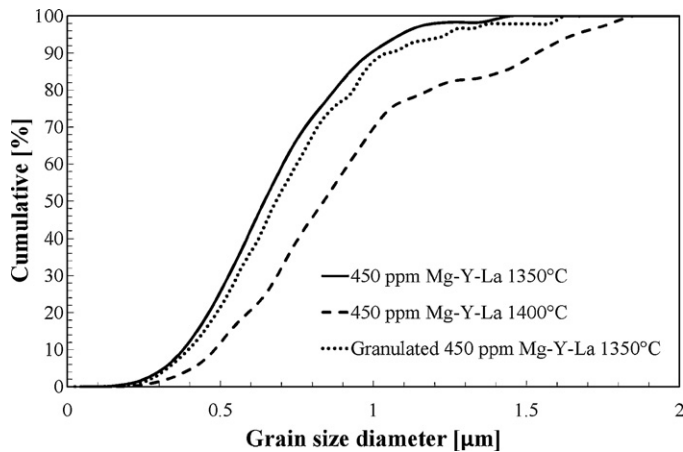


Fig. 12. Cumulative volume grain size distribution curves for the 450 ppm ( $\text{Mg}^{2+}$ ,  $\text{Y}^{3+}$ ,  $\text{La}^{3+}$ )-doped samples sintered from loose powder at 1350 °C and 1400 °C as well as from the sample sintered from C3 granules. Increasing sintering temperature increases the distribution range and favors multi-modal grain size distributions, as indicated by the plateaus in the distribution curves.

for 48 h with 1 mm pure alumina balls in a plastic jar, however, improves the RIT from 46.7% to 51.7%. This could be linked to (1) powder agglomeration through PAA bridging<sup>46</sup> or (2) configurational changes of PAA upon complexation,<sup>47</sup> both potentially affecting the slurry homogeneity and rheological properties. The latter, through speciation reactions,<sup>47</sup> could also potentially affect the decomposition reactions during binder burnout. Thus rolling could affect the homogeneity of the green body and thereby affect the residual porosity (or grain growth). The remaining 5% RIT difference compared to the loose powder could also be due to another process—most likely incomplete binder burnout as discussed above. In fact, the low atmospheric pressure of oxygen required for PECS in graphite molds renders the process highly sensitive to any organic residues due not only to fast sintering, leaving little time for pyrolysis, but also to the limited oxygen available for decomposition reactions to take place. Although binder burnout could be potentially optimized, the current results demonstrate the successful use of dry pressing of granulated powders for transparent ceramic applications.

The tendency for bi- or multi-modal grain size distributions to develop (Fig. 12) from sintering of loose powder, as observed from the tails of the distribution curves, is not improved by uniaxial pressing of granulated powders. For loose powder, this tendency is believed to result from inhomogeneous powder packing caused by agglomeration of the powder during freeze drying (without organic additives), as illustrated in Fig. 13. The use of additives such as PAA during freeze granulation is believed to prevent agglomeration, and the inhomogeneous powder packing resulting in grain size distribution broadening may result from the uniaxial pressing. Since the powder volume load in the granules is low and the total organic additive content minimized, GB formation by cold isostatic pressing (CIP) is difficult. GB formation by uniaxial pressing followed by CIP should therefore be investigated in addition to different binder burnout routes to optimize the potential of freeze granulation techniques for transparent ceramic applications. Higher solid loading by further optimization of the powder

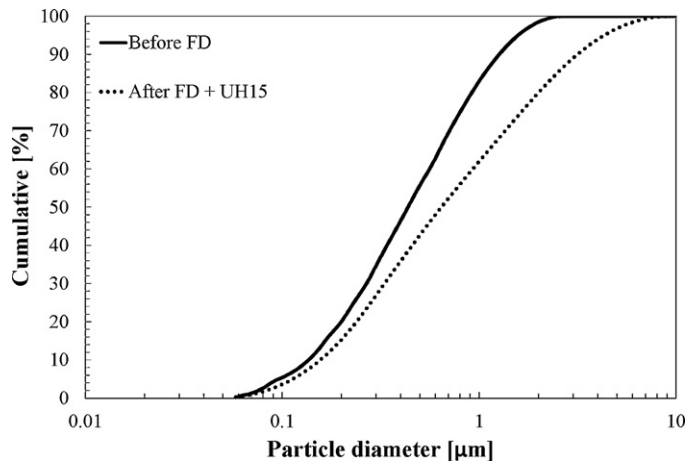


Fig. 13. Cumulative powder size distribution curves, before and after freeze drying (FD). Powder agglomeration occurs during freeze drying which cannot be fully recovered by a 15-min ultrasonic-horn treatment (UH15).

dispersion is also desired. This could perhaps be achieved by using dispersants other than PAA which are less sensitive to the ionic concentration of the dopant solutions, such as the comb-like polymers used in cement dispersion.<sup>48</sup> This would allow CIP methods to be used directly and further improve GB homogeneity and resulting transparency.

#### 4. Conclusion

Powder granulation and dry pressing for transparent ceramic applications has been demonstrated to be a promising alternative to loose powder sintering, providing real in-line transmittance values competitive with those obtained from much slower and more fastidious colloidal green body processing routes. Careful control of the rheological behavior permitted freeze granulation of alumina slurries in spite of the required dopant nitrates having a negative effect on the viscosity and yield stress. The freeze granulation RITs compete with other loose powder sintering results found in the literature,<sup>8,19</sup> despite the slightly lower real in-line transmittance values from PECS sintering of green bodies prepared from granulated powders compared to loose powders (52% instead of 57%) here. With future work focusing on the use of smaller starting powders, better powder dispersion for higher solid loadings, binder burnout—a crucial step for PECS—and green body pressing, freeze granulation shows strong promise as a simple powder processing route for industrial scale development for transparent ceramic fabrication.

#### Acknowledgments

The Swiss National Science Foundation is acknowledged for its support through grant no. 200021-122288/1. Céramet SA (Bôle, Switzerland) is acknowledged for the sample polishing. We also appreciate the EM facility support from the Knut and Alice Wallenberg Foundation.

## References

1. Apetz R, van Bruggen MPB. Transparent alumina: a light-scattering model. *Journal of the American Ceramic Society* 2003;**86**(3):480–6.
2. Krell A, Hutzler T, Klimke J. Transmission physics and consequences for materials selection: manufacturing, and applications. *Journal of the European Ceramic Society* 2009;**29**(2):207–21.
3. Pecharomán C, Mata-Osoro G, Díaz LA, Torrecillas R, Moya JS. On the transparency of nanostructured alumina: Rayleigh–Gans model for anisotropic spheres. *Optics Express* 2009;**17**(8):6899–912.
4. Peelen JGJ, Metselaar R. Light scattering by pores in polycrystalline materials: transmission properties of alumina. *Journal of Applied Physics* 1974;**45**(1):216–20.
5. Bohren CF, Huffman DR. *Absorption and Scattering of Light by Small Particles*. Chichester, UK: Wiley; 1998.
6. Braun A, Falk G, Clasen R. Transparent polycrystalline alumina ceramic with sub-micrometre microstructure by means of electrophoretic deposition. *Materialwissenschaft Und Werkstofftechnik* 2006;**37**(4):293–7.
7. Grasso S, Kim BN, Hu C, Maizza G, Sakka Y. Highly transparent pure alumina fabricated by high-pressure spark plasma sintering. *Journal of the American Ceramic Society* 2010;**93**(9):2460–2.
8. Kim BN, Hiraga K, Morita K, Yoshida H, Kagawa Y. Light scattering in MgO-doped alumina fabricated by spark plasma sintering. *Acta Materialia* 2010;**58**(13):4527–35.
9. Krell A, Blank P, Ma H, Hutzler T, van Bruggen MPB, Apetz R. Transparent sintered corundum with high hardness and strength. *Journal of the American Ceramic Society* 2003;**86**(1):12–8.
10. Krell A, Klimke J, Hutzler T. Advanced spinel and sub-m  $\text{Al}_2\text{O}_3$  for transparent armour applications. *Journal of the European Ceramic Society* 2009;**29**(2):275–81.
11. Stuer M, Zhao Z, Aschauer U, Bowen P. Transparent polycrystalline alumina using spark plasma sintering: effect of Mg, Y and La doping. *Journal of the European Ceramic Society* 2010;**30**(6):1335–43.
12. Wang C, Zhao Z. Transparent  $\text{MgAl}_2\text{O}_4$  ceramic produced by spark plasma sintering. *Scripta Materialia* 2009;**61**(2):193–6.
13. Wei GC. Transparent ceramic lamp envelope materials. *Journal of Physics D: Applied Physics* 2005;**38**(17):3057–65.
14. Wang C, Zhao Z. Transparent polycrystalline ruby ceramic by spark plasma sintering. *Materials Research Bulletin* 2010;**45**(9):1127–31.
15. Kim BN, Hiraga K, Morita K, Yoshida H. Spark plasma sintering of transparent alumina. *Scripta Materialia* 2007;**57**(7):607–10.
16. Krell A, Klimke J. Effects of the homogeneity of particle coordination on solid-state sintering of transparent alumina. *Journal of the American Ceramic Society* 2006;**89**(6):1985–92.
17. Bernard-Granger G, Guizard C. Spark plasma sintering of a commercially available granulated zirconia powder: I. Sintering path and hypotheses about the mechanism(s) controlling densification. *Acta Materialia* 2007;**55**(10):3493–504.
18. Jiang D, Hulbert DM, Anselmi-Tamburini U, Ng T, Land D, Mukherjee AK. Optically transparent polycrystalline  $\text{Al}_2\text{O}_3$  produced by spark plasma sintering. *Journal of the American Ceramic Society* 2008;**91**(1):151–4.
19. Kim BN, Hiraga K, Morita K, Yoshida H. Effects of heating rate on microstructure and transparency of spark-plasma-sintered alumina. *Journal of the European Ceramic Society* 2009;**29**(2):323–7.
20. Morita K, Kim BN, Hiraga K, Yoshida H. Fabrication of transparent  $\text{MgAl}_2\text{O}_4$  spinel polycrystal by spark plasma sintering processing. *Scripta Materialia* 2008;**58**(12):1114–7.
21. Chakravarty D, Sundararajan G. Effect of applied stress on IR transmission of spark plasma-sintered alumina. *Journal of the American Ceramic Society* 2010;**93**(4):951–3.
22. Zhao Z, Buscaglia V, Bowen P, Nygren M. Spark plasma sintering of nano-crystalline ceramics. *Euro Ceramics* 2004;**264–268**(Viii (pt 1–3)):2297–300.
23. Tsetsekou A, Agrafiotis C, Leon I, Miliatis A. Optimization of the rheological properties of alumina slurries for ceramic processing applications. Part II: Spray-drying. *Journal of the European Ceramic Society* 2001;**21**(4):493–506.
24. Tomas J, Vidal R. The effects of the spray-drying parameters on the manufacturing process of ceramic powders. *Industrial Ceramics* 2006;**26**(2):135–9.
25. Walker WJ, Reed JS, Verma SK. Influence of slurry parameters on the characteristics of spray-dried granules. *Journal of the American Ceramic Society* 1999;**82**(7):1711–9.
26. Lyckfeldt O, Käck D, Rundgren K. Pressing and sintering developments of freeze granulated  $\text{Si}_3\text{N}_4$  materials. *27th International Cocoa Beach Conference on Advanced Ceramics and Composites: B* 2003;**24**(4):331–6.
27. Lyckfeldt O, Rundgren K, Sjöstedt M. Freeze granulation for the processing of silicon nitride ceramics. *Euro Ceramics* 2004;**264–268**(Viii (pts 1–3)):281–4.
28. Yoshida H, Saeki T, Hashimoto K, Fujioka T. Size classification of submicron powder by air cyclone and 3-dimensional analysis. *Journal of Chemical Engineering of Japan* 1991;**24**(5):640–7.
29. Lukasiewicz SJ. Spray-drying ceramic powders. *Journal of the American Ceramic Society* 1989;**72**(4):617–24.
30. Hidber PC, Graule TJ, Gauckler LJ. Competitive adsorption of citric acid and poly(vinyl alcohol) onto alumina and its influence on the binder migration during drying. *Journal of the American Ceramic Society* 1995;**78**(7):1775–80.
31. Nies CW, Messing GL. Effect of glass-transition temperature of polyethylene glycol-plasticized polyvinyl-alcohol on granule compaction. *Journal of the American Ceramic Society* 1984;**67**(4):301–4.
32. Mendelson MI. Average grain size in polycrystalline ceramics. *Journal of the American Ceramic Society* 1969;**52**(8):443–6.
33. Bernard-Granger G, Guizard C, Addad A. Influence of co-doping on the sintering path and on the optical properties of a submicronic alumina material. *Journal of the American Ceramic Society* 2008;**91**(5):1703–6.
34. Stuer M, Bowen P, Cantoni M, Pecharroman C, Zhao Z. Nanopore Characterization and Optical Modeling of Transparent Polycrystalline Alumina. *Advanced Functional Materials* 2012, in press, doi:10.1002/adfm.201200123.
35. Stuer M, Bowen P. Yield stress modeling for doped alumina suspensions for applications in freeze granulation towards dry pressed transparent ceramics. *Advances in Applied Ceramics* 2012, in press, doi:10.1179/1743676111Y.0000000061.
36. Aschauer U, Burgos-Montes O, Moreno R, Bowen P. Hamaker 2: A toolkit for the calculation of particle interactions and suspension stability and its application to mullite synthesis by colloidal methods. *Journal of Dispersion Science and Technology* 2011;**32**(4):470–9.
37. Chen HYT, Wei WCJ, Hsu KC, Chen CS. Adsorption of PAA on the  $\alpha\text{-Al}_2\text{O}_3$  surface. *Journal of the American Ceramic Society* 2007;**90**(6):1709–16.
38. Flatt RJ, Bowen P. Yodel: a yield stress model for suspensions. *Journal of the American Ceramic Society* 2006;**89**(4):1244–56.
39. Juang RS, Liang JF. Equilibrium studies for the interaction of aqueous metal-ions and polyacrylic-acid by a batch ultrafiltration method. *Journal of Membrane Science* 1993;**82**(1–2):163–74.
40. Roma-Luciw R, Sarraf L, Morcellet M. Complexes of poly(acrylic acid) with some divalent: trivalent and tetravalent metal ions. *European Polymer Journal* 2001;**37**(9):1741–5.
41. Sun J, Bergstrom L, Gao L. Effect of magnesium ions on the adsorption of poly(acrylic acid) onto alumina. *Journal of the American Ceramic Society* 2001;**84**(11):2710–2.
42. Hackley VA. Colloidal processing of silicon nitride with poly(acrylic acid). I. Adsorption and electrostatic interactions. *Journal of the American Ceramic Society* 1997;**80**(9):2315–25.
43. King AG. Ceramic technology and processing: a practical working guide. In: *Materials science and process technology series*. William Andrew Inc.; 2001.
44. Lewis JA. Binder removal from ceramics. *Annual Review of Materials Science* 1997;**27**:147–73.
45. Baklouti S, Bouaziz J, Chartier T, Baumard JF. Binder burnout and evolution of the mechanical strength of dry-pressed ceramics containing poly(vinyl alcohol). *Journal of the European Ceramic Society* 2001;**21**(8):1087–92.

46. Hackley VA. Colloidal processing of silicon nitride with poly(acrylic acid): II. Rheological properties. *Journal of the American Ceramic Society* 1998;**81**(9):2421–8.
47. Montavon G, Rabung T, Geckeis H, Grambow B. Interaction of Eu(III)/Cm(III) with alumina-bound poly(acrylic acid): sorption, desorption, and spectroscopic studies. *Environmental Science & Technology* 2004;**38**(16):4312–8.
48. Houst YF, Bowen P, Perchea F, Kauppib A, Borgetc P, Galmichec L, et al. Design and function of novel superplasticizers for more durable high performance concrete (superplast project). *Cement and Concrete Research* 2008;**38**(10):1197–209.